Appl Phys B (2011) 102: 433–442
DOI 10.1007/s00340-011-4410-x

Applied Physics B
Lasers and Optics

Feedback control of a single atom in an optical cavity

A. Kubanek · M. Koch · C. Sames · A. Ourjoumtsev · T. Wilk · P.W.H. Pinkse · G. Rempe

Received: 30 July 2010 / Revised version: 3 November 2010 / Published online: 12 February 2011

Abstract We discuss feedback control of the motion of a single neutral atom trapped inside a high-finesse optical cavity. Based on the detection of single photons from a probe beam transmitted through the cavity, the position of the atom in the trap is estimated. Following this information, the trapping potential is switched between a high and a low value in order to counteract the atomic motion. This allowed us to increase the storage time by about one order of magnitude. Here, we describe the technical implementation of the feedback loop and give a detailed analysis of its limitations as deduced from Monte-Carlo simulations. We also discuss different strategies to further improve the performance of the feedback.

1 Introduction

Only half a century ago Schrödinger doubted that it might ever be possible to do experiments with single particles [1]. The last decades, however, have taught us that this scepticism was unjustified. In particular the development of ion traps [2, 3] and the invention of laser cooling [4–6] made the manipulation of single particles possible. Nowadays, the internal and external degrees of freedom of single particles can be controlled for various applications ranging from precision measurements and time standards [7, 8] to quantum information processing [9]. Here, we concentrate on the external degrees of freedom. More precisely, we aim to observe a single neutral atom moving in a weekly confining optical trap and to steer it into a desired direction by applying a force which depends on the outcome of the observation.

Observing a single atom with high spatial and temporal resolution is not straightforward. It requires either a large numerical-aperture lens or, better, a technique where the information about the atomic trajectory is contained in a well defined light mode. The latter situation can be achieved in cavity quantum electrodynamics (QED) [10]. The advantage of cavity QED comes from the fact that the coupling of the atom to the mode of an optical cavity enhances the rate of spontaneous emission into the mode by means of the Purcell effect. Moreover, if the atom is probed via the cavity mode and the coupling between atom and cavity mode is strong, as in our experiment, this leads to a drastic change in the cavity transmission. As a consequence, the information about the atom is contained in the mode defined by the optical cavity. The absence or presence of photons in this mode can then easily be monitored by means of sensitive light detectors. Position information originates from the spatial structure of the cavity mode, a standing wave along the cavity axis with a Gaussian transverse profile. These elements have already been implemented about a decade ago in order to observe in real time the motion of single neutral atoms inside a high-finesse optical cavity [11, 12].

The next logical step is to actively control the motion of the atom using the knowledge about its motion [13–17],

A. Kubanek (✉) · M. Koch · C. Sames · A. Ourjoumtsev · T. Wilk · P.W.H. Pinkse · G. Rempe
Max-Planck-Institut für Quantenoptik, Hans-Kopfermann-Str. 1, 85748 Garching, Germany
e-mail: kubanek@fas.harvard.edu

Present address:
A. Ourjoumtsev
Laboratoire Charles Fabry, Institut d'Optique, CNRS, Univ. Paris-Sud, Campus Polytechnique, RD 128, 91127 Palaiseau cedex, France

Present address:
P.W.H. Pinkse
MESA+ Institute for Nanotechnology, University of Twente, P.O. Box 217, 7500 AE Enschede, The Netherlands

with the goals to better localize the atom inside the cavity mode and to keep the atom trapped for a longer time. In contrast to feedback control of an ion in a Paul trap [18], both the anharmonicity of the trapping potential and the unpredictability of the atomic motion, stemming from random spontaneous-emission recoil kicks, as well as the interaction of the atom with the near-resonant cavity light field impose high demands on the reaction time of the feedback loop. In fact, a sufficiently fast and reliable feedback algorithm has been successfully implemented only very recently [19].

In general, a feedback loop consists of three major elements. First, a measurement of the parameter which one likes to control has to be performed. Second, based on this observation one needs to make a decision on how to react on the system. Third, the loop has to be closed by actuating on the system. In our experiment, where we want to control the motion of a single atom held in an intracavity dipole trap, these three steps are implemented as follows. We observe the motion of the single atom inside the cavity via the intensity of a probe beam transmitted through the cavity. A decreasing or increasing photon flux indicates whether the atom is moving towards or away from the cavity axis. This change in transmission is processed in a real-time processor, which switches the potential depth of the intracavity dipole trap according to the feedback protocol either to a high or a low value actuating the atomic motion. To increase the storage time of the atom, the dipole potential is increased for an atom moving away from the cavity axis, making it harder for the atom to escape from the trap, whereas it is switched to a low value when the atom starts moving towards the cavity axis, such that it cannot gain much kinetic energy.

All elements of the feedback loop, namely observing, processing and actuating, need to be faster than the time scale on which the atomic motion becomes unpredictable. In our case this time scale is as short as one oscillation period ($\approx$200 µs) of the atom in our weakly confining intracavity trap [19]. In the following, we will detail how the feedback scheme is implemented. Section 2 gives a brief overview of the experimental setup, introduces the different parameter regimes and then concentrates on the implementation of the real-time control. In Sect. 3 Monte-Carlo simulations give important insight into the physics of the feedback control. Section 4 details different improvements of the feedback and discusses new strategies. Finally, Sect. 5 gives a short summary of the work with an outlook on future directions.

2 The strongly coupled atom–cavity system

2.1 Experimental setup

The heart of the experiment is an optical cavity of finesse $\mathcal{F} \approx 440\,000$, with mode waist $w_0 = 29$ µm and length $l = 123$ µm. We use ^{85}Rb atoms and are working in the parameter regime of strong coupling, where the maximal atom–cavity coupling $g_{\max}/2\pi = 16$ MHz exceeds the cavity-field decay rate $\kappa/2\pi = 1.25$ MHz and the atomic polarization decay rate $\gamma/2\pi = 3$ MHz. The strong coupling regime is essential here, since in this case the probe-beam transmission changes significantly due to the new eigenfrequencies of the coupled system when an atom enters the cavity mode.

We use different modes to trap the atom, probe its motion and actuate its trajectory. An overview over the different lasers and employed cavity modes is shown in Fig. 1. To observe the atomic motion, a titanium-sapphire laser at 780 nm (TiSa 780) tuned close to the cycling transition of the D_2 line of ^{85}Rb is coupled to a TEM_{00} mode of the cavity and acts as a probe beam. Trapping of the atom is achieved by an external cavity diode laser (ECDL 785) running at 785 nm which is also coupled into a TEM_{00} mode of the cavity. It is detuned by 2 free-spectral ranges (FSR) from the probe laser such that their antinodes coincide in the center of the cavity. The ECDL 785 is used to stabilize the cavity length and acts as a red-detuned standing wave dipole trap. With trapping frequencies on the order of a few hundred kHz, the axial confinement is much stronger than the radial confinement where the trapping frequencies are about two orders of magnitude smaller. Due to the low signal, we are only able to observe the radial motion in real-time, and consequently our feedback scheme only acts on the radial motion.

In principle, one could switch the depth of the red-detuned dipole laser to actuate the atomic motion. However, this has certain disadvantages. First, switching the red-detuned dipole potential changes the Stark shift and therefore the atom–cavity detuning. As this affects the transmission of the atom–cavity system, observation and actuation would not be completely independent. Second, the switching will also affect the axial motion, and since it occurs randomly with respect to the axial motion, we expect heating in this direction. Third, because of the radial symmetry of the TEM_{00} mode the angular momentum is conserved, which could potentially limit the performance of the feedback.

All these difficulties can be overcome by using an additional repulsive, torus-shaped potential to steer the atomic motion in the radial direction. It is generated by coupling a diode laser at 775 nm (ECDL 775) to both, a TEM_{10} and a TEM_{01} mode of the cavity. The resonance frequencies of the two modes are split by about 6 MHz allowing to control the intensity of either one separately [20]. As these modes are blue-detuned by two FSR with respect to the probe laser, their antinodes overlap with the antinodes of the probe and the red-detuned trapping mode in the axial center of the cavity, providing an additional radial confinement for the trapped atom. For an atom that is well localized in the radial direction, the toroidal trap has little effect on its axial

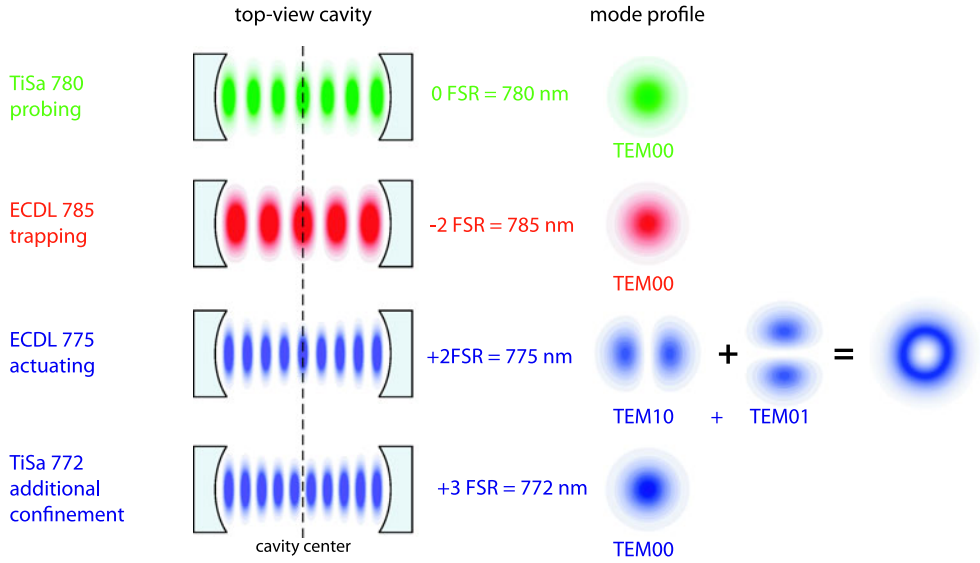

Fig. 1 Employed cavity modes. The atom–cavity system is probed with light at 780 nm, close to the D_2-line of ^{85}Rb. The red-detuned dipole trap (ECDL 785, TEM_{00}) serves to hold the atom inside the cavity mode. To actuate the atomic motion a blue-detuned torus-shaped mode (ECDL 775, $\mathrm{TEM}_{10} + \mathrm{TEM}_{01}$) is used. The red-detuned dipole trap and the blue-detuned toroidal potential are both 2 free-spectral ranges (FSR) apart from the probe mode (in positive and negative direction, respectively), so that their antinodes all coincide in the axial center of the cavity. In some experiments additional axial confinement is realized by another blue-detuned laser at 772 nm, 3 FSR apart from the probe mode

motion. In addition, due to its repulsive potential it induces only a small Stark shift of the atomic transition. Moreover, when switching the intensity either to high or to low values for a stronger or for a weaker confinement of the atom, respectively, the Stark shift does not change much as long as the atom stays close to the cavity axis. By changing the intensity balance between the TEM_{10} and the TEM_{01} mode, the radial symmetry of the trapping potential can be broken, i.e., a rotationally symmetric or asymmetric torus potential can be formed.

For some of the experiments, an additional laser at 772 nm (ECDL 772) is coupled into a TEM_{00} mode of the cavity that is blue-detuned by three FSR from the probe laser. Here, the nodes at the center of the cavity overlap with the antinodes of the probe field. As the laser is blue-detuned with respect to the atomic transition, it acts as a repulsive potential increasing the confinement in the axial direction.

To trap single atoms in the cavity, a cloud of cold rubidium atoms is launched from underneath the cavity via an atomic fountain. In prospect of the arriving atoms the intensity of the red-detuned trap is set to a low value (80 nW), and the blue-detuned laser at 775 nm excites only the TEM_{10} mode that is oriented such that its nodal line is vertical, i.e. parallel to the direction of atoms injection. The resulting funnel guides the atoms towards the center of the cavity. Upon arrival of an atom, heralded by a change in the transmission of the probe light, the intensity of the red-detuned trap is increased (170 nW) to trap the atom. In addition, the balance between the blue-detuned TEM_{10} and a TEM_{01} mode is adjusted to a predefined value. Controlled by the feedback routine its intensity is switched between low power (50 nW) and high power (800 nW) as will be discussed in Sect. 2.3.

2.2 Optical information

Before we start to describe the feedback loop, we would like to detail here how we observe the atomic motion and discuss the optimal choice of parameters. The most natural choice of frequencies for observing an atom inside an optical cavity is to have the laser on resonance with both the cavity and the atom. However, for reasons outlined below, it is more favorable to allow for certain detunings. For example, in the experiment presented here we have fixed the atom–cavity detuning to $\Delta_{ac}/2\pi = (\omega_a - \omega_c)/2\pi = 20$ MHz. With this choice we then have to find a suitable detuning between probe laser and cavity $\Delta_c = \omega_l - \omega_c$ (and therefore also between probe laser and atom $\Delta_a = \omega_l - \omega_a$). The idea is to find a parameter regime where a high contrast is achieved in the transmission signal between a well and a badly coupled atom. Towards this end, we briefly review how the cavity transmission depends on the detunings and the atom–cavity coupling constant. For weak driving, the transmission spectrum of the strongly coupled atom–cavity system follows

$$T = \frac{\kappa^2}{\Delta_c^2 + \kappa^2} \frac{1}{(1-\nu)^2}, \tag{1}$$

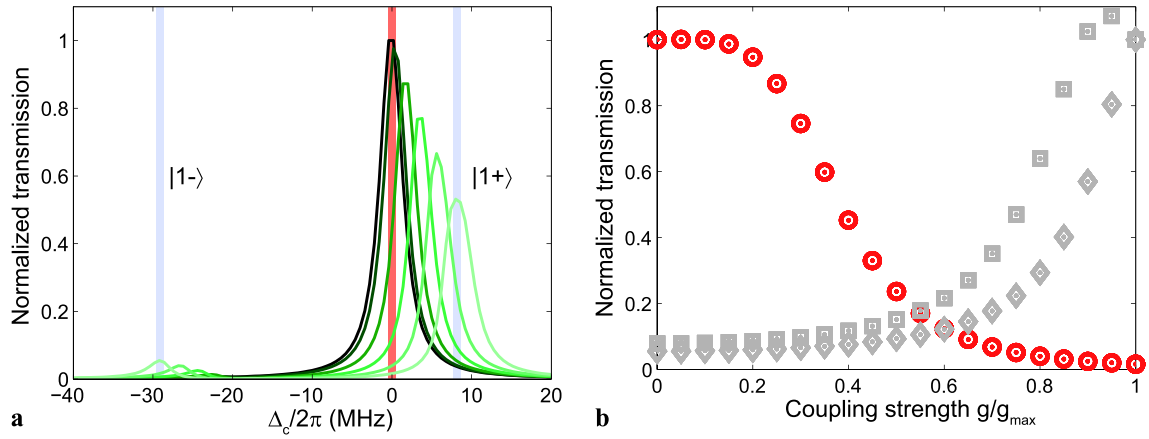

Fig. 2 Observation possibilities. (**a**) Calculated transmission versus laser-cavity detuning Δ_c for a fixed atom–cavity detuning $\Delta_{ac}/2\pi = (\omega_a - \omega_c)/2\pi = 20$ MHz. The best contrast between a well-coupled atom (*light green line* for $g/g_{\max} = 1$) and a badly coupled atom (*black line* for $g/g_{\max} = 0$) is achieved on resonance with the empty cavity, i.e. $\Delta_c = 0$, *red area*. A good contrast can also be realized on resonance with the normal modes (*gray areas*). (**b**) Normalized transmission for the three possible observation regions with high contrast as a function of the coupling strength. On resonance with the empty cavity (*red circles*) the transmission drops when $g/g_{\max}$ is increased from 0 to 1 with the best contrast between $0.2 < g/g_{\max} < 0.6$. When measuring on the normal-mode frequencies (*gray squares* for $|1,+\rangle$, *gray diamonds* for $|1,-\rangle$) the best contrast is achieved above 0.6

with $\nu = g^2/[(\Delta_a + i\gamma)(\Delta_c + i\kappa)]$ [21]. Figure 2 illustrates this transmission spectrum for different coupling strengths, g. The black curve corresponds to $g = 0$ while for the other curves the coupling strength is increased in steps of $0.2g_{\max}$ up to a maximum coupling strength of $g_{\max}/2\pi = 16$ MHz (light green line). The coupling strength depends on the atomic position in radial, r, and axial, z, directions via

$$g = g_{\max}\psi(r, z), \tag{2}$$

where $\psi(r, z) = \cos(kz)\exp(-r^2/\omega_0^2)$ is the mode function of the TEM_{00} mode of the probe beam with $\omega_0 = 29$ μm the mode waist. The transmission spectrum shows a single Lorentzian-shaped resonance for $g = 0$, the empty-cavity resonance. When g is increased, two transmission lines appear, the so-called normal modes. The asymmetry of the spectrum arises from the atom–cavity detuning. It is straightforward to identify three frequency regions which are suitable to observe the atomic motion. One is to have the frequency of the probe laser on resonance with the empty cavity (red region). The other two are to have the laser on resonance with one of the normal modes (two gray regions). The largest contrast is found on resonance with the empty cavity. There, the overall count rate is the highest, which increases the signal-to-noise ratio allowing for a short measurement time. This region is particularly useful for the observation of an atom which attempts to leave the cavity as then the transmission increases by a factor of 70 when g changes from $g_{\max}$ to 0. In contrast, on resonance with the normal modes the transmission increases with increasing coupling strength by a factor of 18 on the lower-frequency normal mode (state $|1,-\rangle$ at a detuning of $\Delta_c/2\pi = -29$ MHz) and by 14 on the higher-frequency normal mode (state $|1,+\rangle$ at a detuning of $\Delta_c/2\pi = 8$ MHz). For pump frequencies between the normal modes but away from the empty-cavity resonance, the transmission signal is a non-monotonic function of the coupling strength and therefore not appropriate for feedback.

To further analyze the two possible frequency regions for monitoring the atomic motion, the relative transmission is plotted as a function of $g/g_{\max}$ in Fig. 2b). The steeper the slope the more sensitive we are to the atomic position. On resonance with the empty cavity the highest sensitivity is obtained for $0.2 < g/g_{\max} < 0.6$, while the transmission is only marginally sensitive to changes of g when the atom is very well localized. On resonance with the normal modes (gray squares corresponds to transitions to state $|1,+\rangle$ and gray diamonds to those to $|1,-\rangle$) the best contrast is achieved for $g/g_{\max} > 0.6$. For these parameters the photon flux is more sensitive to well-coupled atoms.

Before choosing suitable frequencies, one has to consider that the feedback process only acts on the transverse motion of the atom. The axial motion, on the other hand, is affected by cavity-assisted light forces which, depending on the frequencies, can lead to cooling or heating [22]. Laser frequencies around the empty-cavity resonance allow for fluctuations in the detunings without entering a strong heating regime. Even more important, a laser on resonance with the empty cavity provides strong axial cooling of the atom. In contrast, near the normal modes heating regions are in close proximity. Hence, a stable atom–cavity detuning is crucial when measuring on the normal modes. This is difficult to achieve due to the position-dependent Stark shift of the atomic transition inside the dipole trap. Therefore, we

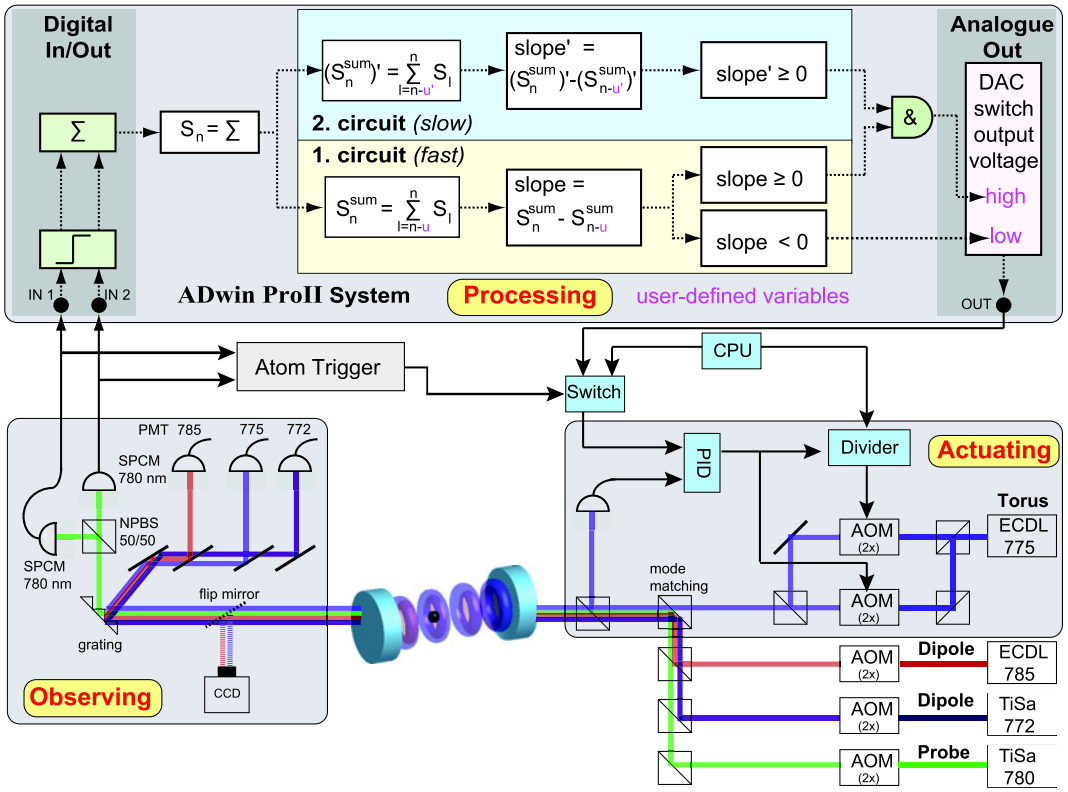

Fig. 3 Scheme of the experimental setup. For simplicity only the real-time computing system and the connected devices are displayed, see text for details. Frequency and power stabilization, as well as cavity locking are omitted

chose to operate the laser close to resonance with the empty cavity.

2.3 Real-time control

A schematic of the control loop is shown in Fig. 3. As discussed above, the feedback loop can be divided into three steps, observing, processing and actuating. The observation of the atomic motion is done by monitoring the transmitted probe-beam intensity. An optical grating behind the cavity separates the probe beam and all dipole trap beams from each other. The various dipole lasers transmitted through the cavity are directed towards photomultiplier tubes (PMTs) observing their intensities. All lasers are sent in double-pass configuration (2×) through acousto-optical modulators (AOMs), which allow for fine tuning of their frequency and amplitude. The probe laser (1 pW) carrying the information about the atomic position is detected by two single photon counting modules (SPCMs) from Perkin&Elmer (AQR-13). The overall detection efficiency including all losses amounts to $\eta = 0.05$. The SPCMs emit short digital pulses (≈30 ns), whose rising edges correspond to the photon arrival times.

The next step in the feedback loop is the processing of the acquired information. Once an atom is trapped in the red dipole trap, the feedback routine is triggered by switching (Switch) the control of the blue-detuned torus power from a computer-controlled measurement sequence (CPU) to the real-time processor (ADwin ProII-System). Both SPCM signals are directly processed in the real-time system. The number of detected photons in two successive time intervals are compared. Based on this comparison, we estimate whether the atom is moving towards or away from the cavity axis. By changing the height of the blue-detuned torus-shaped potential barrier, the motion of the atom is actuated.

In more detail, the digital pulses from the SPCMs are fed into the digital channels of a digital in-/output board (DIO, module ProII-DIO32-TiCo RevE03). On this DIO board a field programmable gate array (FPGA) performs an edge detection and counts the number of events Σ since the last query from the host processor (T11 module with ADSP-TS101S TigerSHARC processor). The host processor continuously runs a main cycle enumerated with the index n, which is treating the received data. The repetition time τ at which this cycle is executed depends on its complexity and is a multiple of the inverse clock rate (1/300 MHz) and typically on the order of 1 µs. The nth iteration of the cycle starts by querying the number of clicks $S_n = \Sigma$ counted since the last cycle from the DIO board. In order to increase

the signal-to-noise ratio, a number u of successive values of S_n are summed. The result will be noted as S_n^{sum}. This variable hence reflects the number of photons that has been detected over an interval length of $T = u \times \tau$. In the following T is called exposure time and is typically on the order of ten microseconds. From the integrated number of photon detections S_n^{sum} we subtract the one delayed by u cycles S_{n-u}^{sum}. The difference between these two values yields the change in the count rate, which is called *slope*. Depending on whether the *slope* is positive, negative or zero, a digital-to-analogue converter (DAC) sets the output voltage of an analogue output channel to a predefined high or low value which at the end controls the intensity of the blue-detuned torus potential.

As mentioned above, we want to react as fast as possible on the observed transmission signal of the probe beam. The output signal of the feedback loop is generated for every cycle n, therefore it takes only one cycle period τ to process the received data and to produce an output signal. However, the feedback is delayed due to the integration of the signal over the exposure time T. For a fast reaction time of the feedback, one could think that it would be optimal to keep the exposure time T short, but one has to find a compromise between reacting fast and a sufficiently high signal-to-noise ratio. Since for atoms close to the cavity axis the probe-beam transmission is extremely low, it would be optimal to continuously adapt the exposure time to the available photon flux. As a first step in this direction, we accounted for the changing photon flux by adding a second decision circuit. The first circuit has a short exposure time T_{fast} and allows for a fast reaction when the photon flux is high. Thus, it is responsible for switching the torus trap back to low power, when the atom is returning towards the cavity axis. The second circuit has a longer exposure time T_{slow} for the purpose of increasing the signal-to-noise ratio when the photon flux is low. This is the case for a well-coupled atom in the center of the cavity. The trap is switched back to high power only if both loops register a positive slope.

The repetition time of the main cycle is $\tau = 1.7\,\mu\text{s}$, if only one decision circuit is activated. If both decision circuits are in use, it increases to $\tau = 2.0\,\mu\text{s}$ due to the higher complexity of the algorithm. In that case typical values for u are 5 for the fast and 20 for the slow circuit.

The final part of the feedback loop is the actuation. The output voltage of the real-time computer controls the amplitude of the light of the torus potential, which is the blue-detuned ECDL 775 laser. The symmetry of the torus potential is adjusted by balancing the intensities of the TEM_{01} and TEM_{10} modes. The intensity ratio is set by the CPU, controlling a divider before one of the AOMs. The symmetry is verified by imaging the mode profile on a CCD camera.

3 Monte-Carlo simulations

To understand the performance of the feedback and to find its limitations, we performed Monte-Carlo simulations. In the past, similar simulations have shown very good agreement with spectroscopic measurements which are sensitive to the (time-averaged) position distribution of the atom in the cavity mode [23, 24]. Here, we focus on the optimization of the storage time. We take into account the conservative trapping potential as well as free-space and cavity-induced dissipative forces, momentum diffusion and parametric heating due to intensity fluctuations of the dipole trap. All simulations include only one decision circuit in the feedback loop.

3.1 Feedback strategies

It is evident that a good strategy to keep the atom in the cavity is to increase the potential when the atom is moving away from the cavity axis, which is the case when the transmission signal increases $slope > 0$, and to decrease the potential when the atom moves towards the cavity axis and the signal decreases $slope < 0$. However, it turns out that the correct treatment of the case with $slope = 0$ is essential for a successful implementation of the feedback. Fig. 4a shows the simulated average storage time as a function of the exposure times T for three different feedback strategies. In the first case (blue, solid line), the torus potential is switched high under the condition $slope \geq 0$ and low under the condition $slope < 0$. In the second case (gray, dotted line) the condition for switching to the high (low) potential is $slope > 0$ ($slope < 0$). And finally, in the third case (black, dashed line), the torus potential is switched high for $slope > 0$ and low for $slope \leq 0$.

Even though the difference between these algorithms lies only in handling the case $slope = 0$ and seems rather small, the effect on the storage time is dramatic for short exposure times where the decision process is based on only very few detected photons. We observe that only the first feedback strategy leads to a significant increase of the storage time. Our explanation for this behavior is that atoms which start to move away from the cavity axis produce only a very weak signal (compare Fig. 2). Therefore, it is favorable to switch on the high toroidal potential already when the transmission drops to zero, that is, under the condition $slope = 0$. For longer exposure times, a sufficiently large number of photons is detected per interval, thus eliminating the difference between the three feedback strategies.

It is also obvious from Fig. 4a that the storage time crucially depends on T (blue line). On the one hand, T must be long enough to gather enough information about the atomic motion. On the other hand, it must be shorter than one quarter of an oscillation period to react in phase with

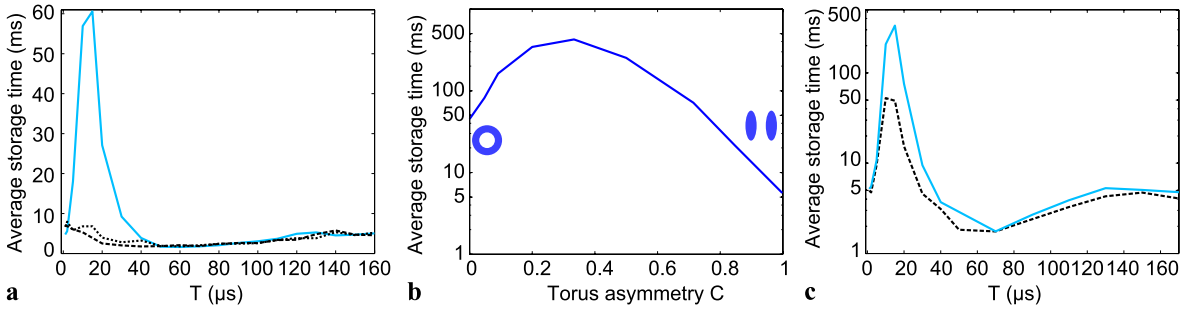

Fig. 4 Monte-Carlo simulations. (**a**) Three different feedback strategies are tested. Here, we assumed an overall detection efficiency $\eta = 0.05$ and a total dark count rate of 0.5 kHz. A significant increase in the storage time is observed only for switching to a high (low) torus potential for *slope* ≥ 0 (*slope* < 0), respectively (*blue line*). The storage time does not increase for the other two strategies, like switching to high (low) torus potential for *slope* > 0 (*slope* < 0) (*gray dotted line*) or for *slope* > 0 (*slope* ≤ 0) (*black dashed line*). (**b**) Influence of the torus asymmetry on the storage time. This improves from ≈ 5 ms for a TEM_{01} mode ($C = 1$) by a factor of 10 for a perfectly symmetric torus ($C = 0$). A further increase by another factor of 10 is achieved when the symmetry of the torus potential is broken for $C \approx 0.2$, ($\eta = 0.03$, dark count rate 0.5 kHz). (**c**) Influence of the noise-photon count rate on the average storage time. If we include the noise count rate of ≈7.5 kHz from our experiment (*black dashed line*), the average storage time decreases by a factor of 10 compared to the case when we take only detector dark counts (0.5 kHz) into account (*blue solid line*)

the atomic oscillation [19]. The simulation shows maximal storage times of almost 60 ms at an exposure time of approximately 15 μs which will be used in the following, if not stated differently.

3.2 Radial symmetry

Since the TEM_{00} mode we are using to probe the atomic motion is radially symmetric, we are only sensitive to the radial motion of the atom and not to its azimuthal component. In addition, the simulations presented above have assumed a radially symmetric torus potential, i.e. a balanced superposition of the TEM_{01} and the TEM_{10} mode, which preserves the angular momentum of the atomic motion. This suggests that our feedback tends to force the atoms on circular trajectories resulting in a constant transmission through the cavity and, hence,the feedback is no longer effective.

This unwanted effect can be overcome by unbalancing the intensities of the TEM_{01} and TEM_{10} modes, thus breaking the radial symmetry. In Fig. 4b we have plotted the average storage time as a function of the symmetry of the torus potential defined by the contrast $C = (I_{01} - I_{10})/(I_{01} + I_{10})$, where I_{XY} is the intensity of the respective TEM_{XY} mode. A value of 0 corresponds to a perfectly symmetric potential, 1 to a TEM_{01} mode. With an overall photon detection efficiency $\eta = 0.03$ we observe for $C = 0$ a storage time of 50 ms. For $0 < C < 0.6$ an increase of the storage time compared to the symmetric potential is observed with a maximum of about 400 ms. Therefore, the experiments are performed with an asymmetric torus potential with a contrast of $C = 0.2$ corresponding to a TEM_{01} mode 50% stronger than the TEM_{10} mode.

3.3 Signal-to-noise ratio

A major issue is the signal-to-noise ratio of the detected photon flux. As the experimentally observed photon flux is as low as 0.03 photons per microsecond for a well-coupled atom, it is not only the unavoidable shot noise but also stray light and detector dark counts that influence the performance of the feedback. In Fig. 4c the average storage time is plotted against the exposure time, now using an asymmetric torus potential of $C = 0.2$ like in the experiment (blue, solid line). The only noise source (apart from shot noise) is the total dark count rate of the detectors of 0.5 kHz. However, we will show in the next section that in order to compensate for pumping to a dark hyperfine state, we have to add a repumping laser perpendicular to the cavity axis. Unavoidable clipping of this laser beam off the cavity mirrors causes an increase of noise photons on the detector. Here, we study how this influences the storage time by artificially increasing the rate of noise photons. The black, dashed line in Fig. 4c shows the average storage time with the same parameters as before but with an increased noise level of 7.5 kHz. The maximum average storage time decreases by almost one order of magnitude. We conclude that it is crucial to minimize the noise level on the detectors for a good performance of the feedback.

4 Optimizing the feedback protocol

We now describe how the feedback loop was optimized experimentally using a number of improvement steps, all aiming to further increase the storage time. The experiments were operated at relatively high probe powers, as this is a

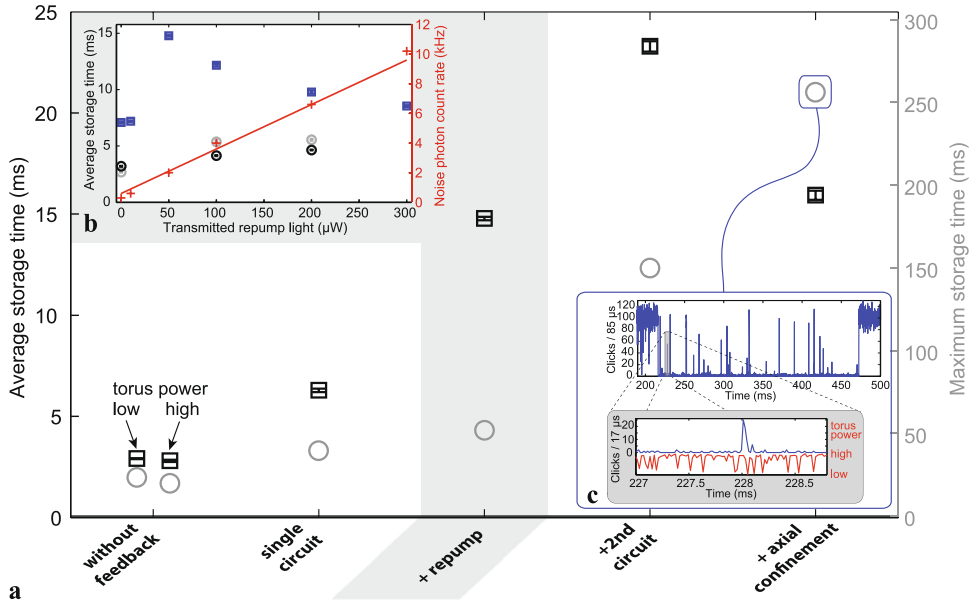

Fig. 5 Experimental improvements. (**a**) The observed storage time increases by successively adding different experimental techniques. For each step the average storage time (*black squares*) is plotted on the left and the storage time of the longest trace (*gray circles*) on the right. As references, measurements without feedback with constant low or high torus potential are shown. Feedback with one decision circuit results already in a clear improvement. Further improvements are achieved by adding a repumping laser, a second decision circuit and an additional axial confinement. (**b**) Influence of the repumping laser power on the storage time. The storage time without feedback increases by about a factor of two in the presence of the repumping light, saturating for powers above 100 μW (*black and gray circles* for high and low torus potential, respectively). When normal feedback is applied (*blue squares*) an increase of the storage time is followed by a decrease for repumping powers above 50 μW due to an enhanced noise-photon rate on the detectors (*red crosses* and *red line*, *right vertical axis*). (**c**) An example of a long trace measured using all improvement steps, where the atom is trapped for about 250 ms. A zoom into the trace is shown with the according switching behavior

promising regime, e.g., to observe quantum nonlinear effects [24, 25]. So far these experiments suffered from short storage times as increasing probe powers lead to an enhanced heating. Figure 5a shows a progression of different improvements in terms of the average (black squares, left axis) and maximum storage time (gray circles, right axis). As a reference the first data point on the left corresponds to a trapping potential kept constant at a high or low level without applying feedback. The average storage time in both cases is below 3 ms with a maximum storage time of 23 ms, limited by radial losses.

4.1 Single-circuit feedback with optimized exposure time

As predicted by the simulations, activating the real-time control of the atom with one decision circuit and an exposure time of $T = 15$ μs significantly increases the storage time by more than a factor of two. The longest trace observed reaches 40 ms.

4.2 Compensation for off-resonant optical pumping

An important loss mechanism of the atom from the cavity is off-resonant optical pumping of the atom into the hyperfine state $5S_{1/2}$, $F = 2$ which is not coupled to the cavity probe field. Imperfect circular polarization can off-resonantly excite the atom to the $5P_{3/2}$, $F' = 3$ level from where it can decay into $5S_{1/2}$, $F = 2$. As feedback operates at moderately high probe powers this loss mechanism becomes more and more important for increasing storage times. It is compensated by an additional repumping laser which resonantly excites the atom from $5S_{1/2}$, $F = 2$ back to $5P_{3/2}$, $F = 3$. This repumping laser is aligned perpendicular to the cavity axis and focused between both mirrors. Clipping of the beam off the edges of the cavity mirrors is unavoidable due to the geometry of the cavity setup, leading to light scattering into the cavity mode and an increased noise-photon rate on the detectors. The photon count rate as a function of the repumping laser power is shown in Fig. 5b (red crosses, right axis). The count rate of noise photons on the SPCMs increases linearly with increasing repumping power (red line).

In Fig. 5b the average storage time is shown as a function of the repumping power on the left vertical axis. When no feedback is applied (black or gray circles for torus power high or low, respectively) the storage time increases by roughly a factor of two. Already a repumping intensity of 100 μW is sufficient to saturate the repumping transition. From the increase in the storage time we can estimate that

the additional loss rate due to off-resonant pumping into the $5S_{1/2}$, $F = 2$ hyperfine ground state is between 70 Hz and 180 Hz without repumping laser. Simulations suggest a rate of 140 Hz, matching the experimental observations.

Testing the effect of a repumping laser in combination with feedback is more complex since there are two competing mechanisms. On one hand, the storage time increases with increasing repumping power, saturating at a certain intensity. On the other hand, increasing the repumping power raises the noise-photon rate which leads to false decisions in the feedback loop. These counteracting effects are observed in the experiment as shown in the data (blue squares) in Fig. 5b. A maximum of the average storage time is found for a repumping power of 50 μW. When increasing the repumping power further the storage time starts decreasing since the position estimation of the feedback loop is perturbed more and more by noise photons from scattered repumping light. This implies that if it would be possible to reduce the noise photons we could still gain in average storage time.

4.3 Second decision circuit

The optimal exposure time T depends on the available photon flux corresponding to the actual atom–cavity coupling strength. The feedback protocol would improve further by dynamically adjusting T to the current position of the atom in the cavity mode. The main problem arises when the atom is well coupled and the flux of information is extremely low. As a first step to account for the dynamics of the changing photon flux, a second decision circuit with a longer exposure time T_{slow} is added for an improved position estimation. The exposure time of the fast circuit is now $T_{\text{fast}} = 10$ μs and of the slow circuit $T_{\text{slow}} = 40$ μs. To switch the torus trap to low power, the outcome of only the fast circuit is sufficient. But for switching to high power, both circuits need to register a positive or constant slope. Then, the atom is likely to be close to the cavity axis and therefore the photon flux is low. The second circuit helps to increase the signal-to-noise ratio in this situation and to improve the timing of the switching process. With this improvement, the average storage time increases to about 24 ms and the longest trapping times exceed 150 ms.

4.4 Axial confinement

Once radial losses are reduced by feedback control, losses along the axial directions should start to play a role. In order to minimize them, additional axial confinement is provided by the blue-detuned TEM_{00} mode at 772 nm. The nodes of the 772 nm mode coincide with the antinodes of the 780 nm probe beam at the center of the cavity, compare Fig. 2. But for increasing distance from the cavity center along the axis the different wavelengths cause a mismatch. In these regions the atom is pushed out of the probe beam and the feedback does not work properly resulting in a reduced average storage time of about 16 ms, as shown in Fig. 5a. However, the additional axial confinement also results in an increase of the maximal storage time to about a quarter of a second for atoms entering the cavity close to the axial center. An example trace of an atom stored for a quarter of a second with the corresponding switching behavior of the feedback loop is shown in Fig. 5c.

5 Summary and outlook

In conclusion, we have given a detailed description of the technical realization of real-time feedback control of a single neutral atom in an optical cavity. Extended storage times of the atom are observed when real-time feedback is applied, demonstrating the power of this technique. However, to compete with state-of-the-art laser cooling, storage times on the order of a second are desirable. Predicted average storage times of about 400 ms in simulations with realistic parameters brings this goal into reach.

To improve the localization of the atom further, feedback could be applied on resonance with one of the normal modes. In this regime the transmission is most sensitive to very well-coupled atoms. Here, the algorithm has to be inverted as the presence of an atom now causes an increase in the transmission. Since any Stark shift would result in shifting the system across heating regions, the blue-detuned torus trap is an ideal actuator for this kind of experiment.

The observed increase of the storage time of the atom in the cavity is a strong evidence for the cooling of the atom. However, it would be interesting to investigate this cooling mechanism directly. We are currently setting up a new cavity QED experiment to optimize the demands of feedback cooling [26]. Further investigation of feedback cooling could be particularly useful for systems with restricted optical access since no side access is needed to cool an atom in all three dimensions. Also systems with complex geometries like those where atoms are trapped close to a tapered fiber [27] or close to a microtoroid [28] could benefit from feedback cooling.

Acknowledgements We thank Karim Murr for valuable discussions. Financial support from the Deutsche Forschungsgemeinschaft (Research Unit 635), the European Union (IST project AQUTE) and the Bavarian Ph.D. programme of excellence (QCCC) is gratefully acknowledged.

References

1. E. Schrödinger, Br. J. Philos. Sci. **3**, 109 (1952)
2. H. Dehmelt, Rev. Mod. Phys. **62**, 525 (1990)
3. W. Paul, Rev. Mod. Phys. **62**, 531 (1990)
4. S. Chu, Rev. Mod. Phys. **70**, 685 (1998)

5. C.N. Cohen-Tannoudji, Rev. Mod. Phys. **70**, 707 (1998)
6. W.D. Phillips, Rev. Mod. Phys. **70**, 721 (1998)
7. T. Schneider, E. Peik, C. Tamm, Phys. Rev. Lett. **94**, 230801 (2005)
8. C.W. Chou, D.B. Hume, J.C.J. Koelemeij, D.J. Wineland, T. Rosenband, Phys. Rev. Lett. **104**, 070802 (2010)
9. P. Zoller, T. Beth, D. Binosi, R. Blatt, H. Briegel et al., Eur. Phys. J. D **36**, 203 (2005)
10. H. Carmichael, *An Open Systems Approach to Quantum Optics* (Springer, Berlin, 1993)
11. C.J. Hood, T.W. Lynn, A.C. Doherty, A.S. Parkins, H.J. Kimble, Science **287**, 1447 (2000)
12. P.W.H. Pinkse, T. Fischer, P. Maunz, G. Rempe, Nature **404**, 365 (2000)
13. A. Ashkin, J.M. Dziedzic, Appl. Phys. Lett. **30**, 202 (1977)
14. N.V. Morrow, S.K. Dutta, G. Raithel, Phys. Rev. Lett. **88**, 093003 (2002)
15. T. Fischer, P. Maunz, P.W.H. Pinkse, T. Puppe, G. Rempe, Phys. Rev. Lett. **88**, 163002 (2002)
16. T.W. Lynn, K. Birnbaum, H.J. Kimble, J. Opt. B **7**, 215 (2005)
17. D.A. Steck, K. Jacobs, H. Mabuchi, S. Habib, T. Bhattacharya, Phys. Rev. A **74**, 012322 (2006)
18. P. Bushev, D. Rotter, A. Wilson, F. Dubin, C. Becher, J. Eschner, R. Blatt, V. Steixner, P. Rabl, P. Zoller, Phys. Rev. Lett. **96**, 043003 (2006)
19. A. Kubanek, M. Koch, C. Sames, A. Ourjoumtsev, P.W.H. Pinkse, K. Murr, G. Rempe, Nature **462**, 898 (2009)
20. T. Puppe, I. Schuster, A. Grothe, A. Kubanek, K. Murr, P.W.H. Pinkse, G. Rempe, Phys. Rev. Lett. **99**, 013002 (2007)
21. K. Murr, J. Phys. B, At. Mol. Opt. Phys. **36**, 2515 (2003)
22. P. Maunz, T. Puppe, I. Schuster, N. Syassen, P.W.H. Pinkse, G. Rempe, Nature **428**, 50 (2004)
23. P. Maunz, T. Puppe, I. Schuster, N. Syassen, P.W.H. Pinkse, G. Rempe, Phys. Rev. Lett. **94**, 033002 (2005)
24. I. Schuster, A. Kubanek, A. Fuhrmanek, T. Puppe, P.W.H. Pinkse, K. Murr, G. Rempe, Nat. Phys. **4**, 382 (2008)
25. A. Kubanek, A. Ourjoumtsev, I. Schuster, M. Koch, P.W.H. Pinkse, K. Murr, G. Rempe, Phys. Rev. Lett. **101**, 203602 (2008)
26. M. Koch, C. Sames, A. Kubanek, M. Apel, M. Balbach, A. Ourjoumtsev, P.W.H. Pinkse, G. Rempe, Phys. Rev. Lett. **105**, 173003 (2010)
27. E. Vetsch, D. Reitz, G. Sagué, R. Schmidt, S.T. Dawkins, A. Rauschenbeutel, Phys. Rev. Lett. **104**, 203603 (2010)
28. B. Dayan, A.S. Parkins, T. Aoki, E.P. Ostby, K.J. Vahala, H.J. Kimble, Science **319**, 1062 (2008)